Title	Theoretical models for underwater RFID
Authors	Peres, Caroline;Buckley, John;Rather, Nadeem N.;O'Flynn, Brendan
Publication date	2019-10
Original Citation	Peres, C., Buckley, J., Rather, N. and O'Flynn, B. (2019) 'Theoretical Models for Underwater RFID', SENSORCOMM 2019: The Thirteenth International Conference on Sensor Technologies and Applications, Nice, France, 27-31 October, pp. 80-88.
Type of publication	Conference item
Link to publisher's version	https://www.thinkmind.org/index.php?view=article&articleid=sensorcomm_2019_5_10_10065
Rights	© IARIA, 2019
Download date	2024-07-06 05:11:54
Item downloaded from	https://hdl.handle.net/10468/9642

University College Cork, Ireland
Coláiste na hOllscoile Corcaigh

Theoretical Models for Underwater RFID

Caroline Peres, John Buckley, Nadeem Rather, Brendan O'Flynn

Tyndall National Institute

University College Cork

Cork, Ireland

email: caroline.peres@tyndall.ie, john.buckley@tyndall.ie, nadeem.rather@tyndall.ie, brendan.oflynn@tyndall.ie

Abstract—Underwater wireless communications pose challenges due to the characteristics of water as a propagation channel medium. Regardless, it is needed for a range of systems that operate underwater. Commonly used technologies for these use cases (radio-frequency, acoustic and optical communications) are lacking, as they usually suffer from strong attenuation, multipath and propagation delays. In this context, we explore Radio Frequency Identification (RFID) systems underwater and the feasibility of their application. This paper aims to discuss the theoretical transmission models for RFID systems underwater, separating them into near-field systems – which use Magnetic Induction (MI) to communicate – and far-field systems – that transfer data via Radio Frequency (RF). We determine the path loss for each case, explore its value for different system configurations and present preliminary measurements of magnetic field strength.

Keywords–RFID; underwater wireless communications; underwater RFID; near-field communication; magnetic induction.

I. INTRODUCTION

Underwater wireless communications present some challenges due to the channel medium. The underwater environment has different characteristics and phenomena compared to the terrestrial radio propagation channel [1]. Despite these difficulties, underwater wireless communications are needed for underwater systems. Practical applications include seismic activity monitoring, equipment monitoring and control, underwater wireless sensor networks, underwater robots and Underwater Autonomous Vehicles (UAVs), aquaculture and underwater environment monitoring [2][3].

There are three commonly used technologies for underwater communications [1][4][5]. Radio-frequency (RF) communication consists of propagating electromagnetic waves, and it has high data rates at short ranges but suffers from multipath propagation, strong attenuation and Doppler effect [1]. Due to the increasing attenuation for higher frequencies, it requires that systems operate at lower frequencies for longer ranges, which demands large antennas. Acoustic communication makes use of propagating sound waves, which have low attenuation underwater, achieving the longest range. However, this type of communication exhibits high propagation delay due to the speed of sound underwater, suffers from multipath propagation, and is affected by a large delay spread that leads to intersymbol interference. Temperature gradients and ambient noise are also problems for acoustic communications. Another technology is optical communication, that leverages electromagnetic waves in the visible spectrum to transmit data. They have large data rates with low propagation delay.

However, they suffer severe absorption in water and strong backscatter due to suspended particles.

Underwater Radio-Frequency Identification (RFID) is not an extensively explored topic due to the problems outlined above. However, some RFID systems communicate via Magnetic Induction (MI), which could provide an alternative for the existing technologies. In this paper, we want to explore this possibility. We examine the different methods of communication that different RFID systems employ, separating them into two categories: near-field communication and far-field communication. Theoretical mathematical models exist for terrestrial RFID systems, from which the system functionality, communication properties and link budged can be derived. This paper aims to derive similar models for underwater RFID communications, by describing the underwater channel physical properties for near-field and far-field electromagnetic fields by presenting the path loss for each. This can then be used to predict communication range, link budget and channel capacity.

This paper is organised as follows. Section II discusses the related work. In Section III, we give a brief overview of an RFID system and its components. Section IV then presents the model for underwater RFID for near-field and far-field communications. In Section V, we present preliminary results of measurements done of magnetic field strength in free-space and freshwater. Section VI discusses underwater RFID in light of the theory presented and the measurement results. We conclude the paper in Section VII.

II. RELATED WORK

Underwater RFID is not a common topic due to the challenges that the underwater environment poses to RF communications. However, some preliminary work has been done. For example, [6] explores the use of Near-Field Communication (NFC) underwater. Using smartphones and smart cards operating at 13.56 MHz, they tested the read range achieved and the influence of dissolved salts in water in the read range. Another group used Low-Frequency (LF) RFID to track the sediment movements in a beach [7]. Transponders were coupled to pebbles, creating "smart" pebbles that could be detected at up to 50 cm underwater. They were then released into the beach and tracked to map the sediment movement. Systems that use LF RFID underwater can be found in Passive Integrated Transponder (PIT) tags used to uniquely identify fish in fisheries and research [8][9].

The authors in [10] summarised the current understanding of underwater RFID, examining the penetration depth

in freshwater and seawater. However, the model presented is simplified and accounts only for the far-field operation. They also showcase other uses of RFID underwater, such as underwater pipeline monitoring. Other authors have explored MI communications underwater, where the system communicates via induction coupling. [11] provides an overview of the current research findings and challenges for MI. Models for MI can be found in [12]–[16].

III. RFID System

RFID uses electromagnetic fields to identify, track and communicate with electronic data carrying devices (usually called tags) [17]. An RFID system is comprised of a *transponder or tag* that is the object to be identified and a *reader* that reads/writes data from/to the transponder. The tag consists of a coupling element (antenna or coil) and a microchip that stores the data, while the reader has an antenna, a control unit and a radio frequency module.

For data transfer, the reader generates an electromagnetic field to query any transponders in its range. The tag receives the signal via its coupling element, and the energy captured from the electromagnetic field is used to power up the transponder's chip. This chip then sends back the data to the reader via load modulation or backscatter. In general, the transponder is passive (does not contain a power source), and it is powered by the field generated by the reader. There are also semi-active and active devices that have power sources that can power up additional circuitry and extend the range of communication.

IV. RFID Channel Physical Characteristics

The antenna or coil of the RFID reader generates an electromagnetic field. These fields can be described as time-harmonic fields in a lossy medium [18]:

$$\nabla^2 \mathbf{E} = \gamma \mathbf{E} \tag{1}$$
$$\nabla^2 \mathbf{H} = \gamma \mathbf{H} \tag{2}$$

where γ is the propagation constant, with α as the attenuation and β as the phase constants. The wavelength λ is $\lambda = 2\pi/\beta$.

$$\gamma = \alpha + j\beta = \sqrt{j\omega\mu(\sigma + j\omega\varepsilon)} \tag{3}$$

$$\alpha = \omega\sqrt{\mu\varepsilon}\left[\frac{1}{2}\left(\sqrt{1 + \left(\frac{\sigma}{\omega\varepsilon}\right)^2} - 1\right)\right]^{1/2} \quad \left(\frac{Np}{m}\right) \tag{4}$$

$$\beta = \omega\sqrt{\mu\varepsilon}\left[\frac{1}{2}\left(\sqrt{1 + \left(\frac{\sigma}{\omega\varepsilon}\right)^2} + 1\right)\right]^{1/2} \quad \left(\frac{rad}{m}\right) \tag{5}$$

The dielectric permittivity of the medium ε is further defined by $\varepsilon = \varepsilon_r\varepsilon_0$, $\varepsilon_0 = 8.854 \cdot 10^{-12} F/m$ being the permittivity in air and ε_r the relative permittivity of the medium (also known as dielectric constant) that is 81 for water. $\mu = \mu_0 = 4\pi \cdot 10^{-7} H/m$ is the magnetic permeability of the medium, that does not change for non-magnetic media.

The salinity of the water is proportional to the concentration of dissolved salts (chloride, sodium, sulphate, etc.).

The conductivity σ is dependent on temperature, pressure and salinity. In marine water, the conductivity ranges from 2 S/m to 6 S/m, being considered constant 4 S/m in most cases [10]. In freshwater, the considerations are the same. However, the salinity is lower, which means that the conductivity is lower (typically ranging from 30 to 2000 μS/cm) [10]. Due to this high conductivity, Eddy currents are induced within the water, caused by the propagating magnetic field. These Eddy currents are a source of attenuation of the magnetic field.

For the Transverse Electromagnetic Mode to the positive z direction in lossy medium (in this case, water), $\mathbf{E}$ and $\mathbf{H}$ can be derived as [18]:

$$\mathbf{E}(\mathbf{z}) = \hat{\mathbf{a}}_x E_0 e^{-\gamma z} \tag{6}$$
$$\mathbf{H}(\mathbf{z}) = \hat{\mathbf{a}}_y \frac{\gamma}{j\omega\mu} E_0 e^{-\gamma z} \tag{7}$$

For a given antenna, the space that surrounds it can be separated into three regions: (a) a reactive near-field, (b) a radiating near-field and (c) the far-field. There are no abrupt changes at their boundaries [19]. A representation of these regions can be seen in Figure 1.
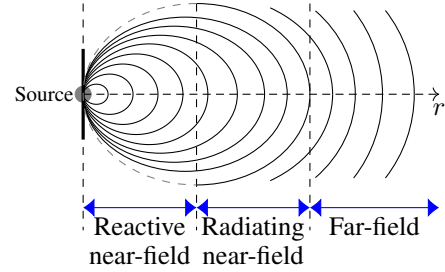

Figure 1. Field regions.

The *Reactive Near-Field* is the space immediately near the antenna where the reactive field predominates (magnetic field). For most antennas, the limit of this region is at $0.62\sqrt{D^3/\lambda}$ [19], where D is the biggest dimension of the antenna. The *Radiating Near-Field* is located between the reactive near-field and the far-field and is the space wherein radiation fields are dominant. The angular field distribution is determined by the distance from the antenna. This field existence depends on the ratio between antenna size D and the wavelength λ: if $D/\lambda \ll 1$ then this region does not exist. The *Far-Field* is the region wherein the electrical and magnetic components of the field become orthogonal to each other as they separate from the antenna and propagate as an electromagnetic wave. The lower boundary of this region is located at $2D^2/\lambda$ for any antenna [18], also considered to be $\lambda/2\pi$ for dipole antennas. According to [17], a good rule of thumb for RFID systems is to place the beginning of the far-field at $\lambda/2\pi$.

The field boundary distance is different for each medium due to the difference in wavelength. Tables I and II show the values for the attenuation coefficient, wavelength and far-field boundary for freshwater and seawater respectively.

Current RFID systems can be separated into two categories: near-field systems that work with inductive coupling due to the dominance of the magnetic field in the near-region, and far-field systems that receive power from the propagating

Frequency	α (Np/m)	λ (m)	z_F (m)
134.2 kHz	$2.81 \cdot 10^{-2}$	$1.66 \cdot 10^{2}$	26.5
13.56 MHz	$4.19 \cdot 10^{-2}$	2.46	0.391
433.92 MHz	$4.19 \cdot 10^{-2}$	$7.68 \cdot 10^{-2}$	$1.22 \cdot 10^{-2}$
915 MHz	$4.19 \cdot 10^{-2}$	$3.64 \cdot 10^{-2}$	$5.79 \cdot 10^{-3}$
2.4 GHz	$4.19 \cdot 10^{-2}$	$1.39 \cdot 10^{-2}$	$2.21 \cdot 10^{-3}$

Frequency	α (Np/m)	λ (m)	z_F (m)
134.2 kHz	1.46	4.32	0.687
13.56 MHz	14.5	0.426	$6.78 \cdot 10^{-2}$
433.92 MHz	65.4	$6.00 \cdot 10^{-2}$	$9.55 \cdot 10^{-3}$
915 MHz	76.5	$3.33 \cdot 10^{-2}$	$5.30 \cdot 10^{-3}$
2.4 GHz	82.4	$1.37 \cdot 10^{-2}$	$2.17 \cdot 10^{-3}$

electromagnetic waves in the far-field [20]. The frequencies used in each region are different. Since the lower frequencies – such as Low Frequency (LF) at around 134.2kHz and High Frequency (HF) at 13.56MHz – have a far-field boundary that is further away, they are mainly used in inductive coupling systems. Higher frequencies are then used mostly in far-field systems.

A. Near-field

In the near-field, the magnetic field created by the reader's antenna induces a voltage in the transponder immersed in this field. This is called *inductive coupling* and the interaction between reader and transponder can be considered as coupled inductors. This method of communication can also be called *Magnetic Induction (MI)*.
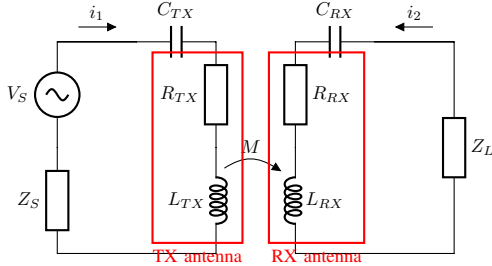

Figure 2. Inductive coupling between reader and transponder.

Consider the equivalent circuit for the inductively coupled system shown in Figure 2. The transmitter antenna is fed by a source with internal impedance Z_S and the receiver antenna is terminated by a load impedance Z_L. The transmitter coil antenna has a impedance of $Z_{TX} = R_{TX} + j\omega L_{TX} + 1/(j\omega C_{TX})$ and the receiver coil antenna is $Z_{RX} = R_{RX} + j\omega L_{RX} + 1/(j\omega C_{RX})$.

Using the two-port network equivalent (Figure 3) and considering an ideal source for V_S, $Z_{11} = Z_{TX}$ and $Z_{22} = Z_{RX}$ are the self-impedances of the coils and $Z_{12} = Z_{21} = j\omega M$ are the mutual impedances due to the coupling.
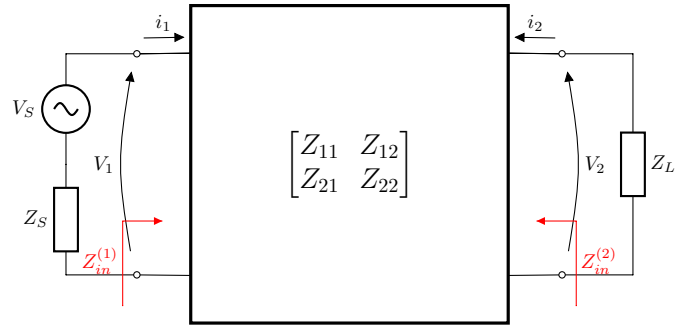

Figure 3. Two-port network equivalent of the system.

$$\begin{pmatrix} V_1 \\ -Z_L I_2 \end{pmatrix} = \begin{bmatrix} Z_{11} & Z_{12} \\ Z_{21} & Z_{22} \end{bmatrix} \cdot \begin{pmatrix} I_1 \\ I_2 \end{pmatrix} \tag{8}$$

The resistance of a coil is $R = N \cdot 2\pi a \cdot R_0$, where N is the number of turns of the coil, a is the diameter of the coil and R_0 is the resistance of a unit of length of the wire used to fabricate the coil. The self-inductance is

$$L = \frac{\mu \pi^2 N^2 a}{l} \tag{9}$$

where l is the length of the coil. In the free space, the magnetic field strength generated by a coil antenna in the near field is [17]:

$$H_0 = \frac{N a^2 I}{2(a^2 + z^2)^{3/2}} \tag{10}$$

The magnetic field magnitude for a lossy medium is then $H = H_0 exp(-\alpha z)$ according to (7). This magnetic field induces a voltage in the tag's coil antenna, given by:

$$U_2 = -N_2 \frac{d\Phi_{21}}{dt} = -M \frac{di_1}{dt} \tag{11}$$

where $\Phi_{21} = \int \mathbf{B} \cdot d\mathbf{S}$ is the magnetic flux through each turn, $\mathbf{B} = \mu \mathbf{H}$ the magnetic field and $\mathbf{S}$ the surface area of the coil. Considering that the reader's and tag's coils are aligned, and using (10):

$$B_z = \left(\frac{\mu N a_1^2 I}{2(a_1^2 + z^2)^{2/3}} \right) e^{-\alpha z} \tag{12}$$

Therefore, the mutual inductance $M = k\sqrt{L_1 L_2}$ is:

$$M = \left(\frac{\mu \cdot \pi \cdot N_1 \cdot a_1^2 \cdot N_2 \cdot a_2^2}{2 \cdot (a_1^2 + z^2)^{3/2}} \right) \cdot e^{-\alpha z} \tag{13}$$

where α is the attenuation constant of the medium.

The transmission power can be defined as the power consumed by the radiation resistance in the reader (transmitter) antenna:

$$P_{TX} = \frac{1}{2} Re(Z_{11}) \cdot |I_1|^2 \qquad (14)$$

The received power is defined as the power consumed in the load:

$$P_{RX}(z) = \frac{1}{2} Re(Z_L) \cdot |I_2|^2 \qquad (15)$$

Using (8) and considering $Z_S \approx 0$, the received power can be written as:

$$P_{RX}(z) = P_{TX} \frac{Re(Z_L)\omega^2 M^2}{Re(Z_{TX})|Z_L + Z_{RX}|^2} \qquad (16)$$

Path loss in decibels (dB) can be defined as:

$$PL = -10 \log_{10} \left(\frac{P_{RX}}{P_{TX}} \right) (dB) \qquad (17)$$

The path loss is a function of the number of turns and radius of both coils and the impedances of the system, as well as the frequency and the distance between reader and tag. The highest amount of power is transferred to the load when its impedance is matched with the impedance of the antenna.

For an example system with a transmitter antenna with 100 turns and 1 m of radius paired with a receiver antenna with 100 turns and 10 cm of radius, both resonant at 134.2 kHz, the path loss in terms of range is shown in Figure 4. The path loss as a function of frequency is shown in Figure 5.
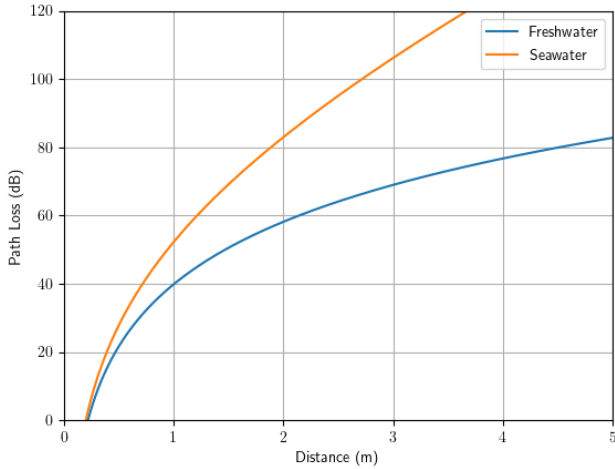

Figure 4. Path loss for an inductively coupled system operating at $f = 134.2$kHz.

The path loss for the MI system increases with the increasing distance between reader and tag. Also, the path loss is higher for seawater due to the higher conductivity of the medium. In freshwater, an increase in frequency decreases the path loss. However, as the frequency increases, the distance from the reader where the border between the near and the far-field is located decreases. This implies that the maximum theoretical range decreases with frequency. We can then conclude that there is an optimal combination of frequency and distance for each application. The decrease in path loss for
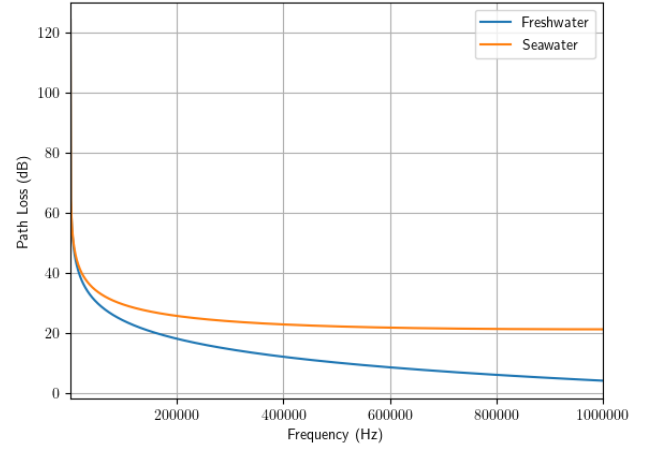

Figure 5. Path loss for an inductively coupled system at range $z = 50$ cm.

higher frequencies is not as significant in seawater. This is due to the higher conductivity, where the attenuation factor is stronger for higher frequencies.

The influence of the number of turns of the transmitter or the receiver coil in the mutual inductance M is linear. Therefore the power received would increase quadratically with the increase in the number of turns. The relationship between the power and radius of the coil is not so straightforward. Figure 6 shows this relationship for a system operating at 134.2kHz with a transmitter antenna with 100 turns and variable radius, with a receiver antenna with 100 turns and 10 cm of radius, at 50 cm of distance between reader and tag.
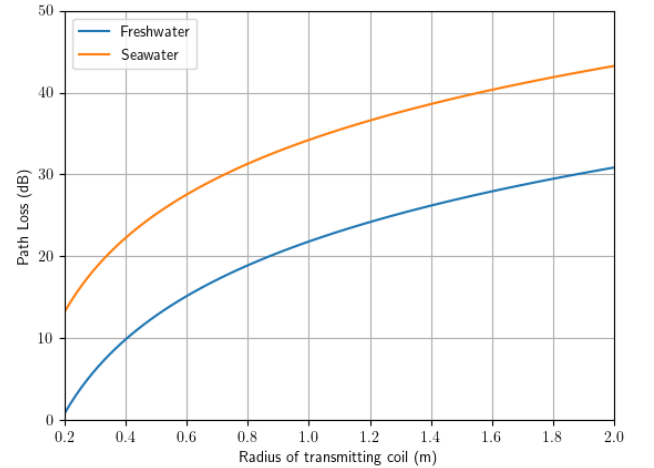

Figure 6. Path loss for an inductively coupled system at range $z = 50$ cm and frequency $f = 134.2$kHz.

A more in-depth model of underwater magnetic induction communication can be found in [13]. The model shown here assumes that the reader and tag coils are oriented in the same direction, with the field strength reaching zero if the angle between coils is 90°. To remove this limitation, the authors in [21] present a model of the Underwater MI channel for a tri-directional coil. To increase the achievable range of MI systems, waveguides can be used [12][22].

Data transmission from tag: When a transponder is located in the magnetic alternating field generated by the reader, the reader 'sees' the transponder as the secondary wing of the transformer. This means that the transponder's impedance is reflected back to the reader as the *transformer impedance Z_T*.

If the transponder antenna impedance changes, this is reflected back to the reader's coil via the reflected impedance Z_T. Therefore, a data stream can be transmitted via modulation of the voltage U_L in the reader's coil (called *Load Modulation*); this can be demodulated by the reader via rectification of the voltage [17]. This is only feasible in the near-field as if the transponder leaves the coupling is lost and the transmission link is not operational anymore.

For an amplitude modulating system, due to the weak coupling between reader and transponder antennas, the voltage fluctuation is orders of magnitude smaller than the voltage provided by the reader. As a direct result, the reader has to integrate a complex circuitry to separate noise from the signal and detect the data stream. On the other hand, if the transponder modulates the signal at a frequency f_S, smaller than the frequency of the magnetic field (f_0), two spectral lines $\pm f_S$ are created and they can be filtered with a band-pass filter and demodulated more easily [20].

B. Far-field

In the far-field, the electromagnetic fields separate completely from the reader's antenna and become propagating waves, no longer retroacting upon the reader's antenna. These waves are captured by the antenna on the transponder. The energy on the antenna is rectified and used to power up the IC. The frequency range commonly used for this type of transmission is the Ultra-High Frequency (UHF) and Microwave.

A linearly polarized plane EM wave propagating in lossy media in the z-direction can be described by the electric field strength E_x:

$$E_x = E_0 e^{j\omega t - \gamma z} \tag{18}$$

With $\gamma = \alpha + j\omega\beta$ as the propagating constant according to (4) and (5).

In [23], the authors propose a review of this model to account for the difference between the theoretical model and the empirical data of attenuation of the radio waves underwater. The experiments show that the signal attenuation at higher distances ($\gg 10m$) is not as strong as predicted. Therefore, they redefine the attenuation constant α as a corrected absorption factor $\alpha\prime$ that matches experimental results closely:

$$\alpha\prime = \left(\frac{\lambda}{\lambda + r}\right) \cdot \alpha \tag{19}$$

Figure 7 shows the difference in the path loss for both models in freshwater and seawater for a system operating at 13.56 MHz.

The radiation power density S is the instantaneous value of the Poynting vector $\mathbf{S} = \mathbf{E} \times \mathbf{H}$. From [18] and considering (7):
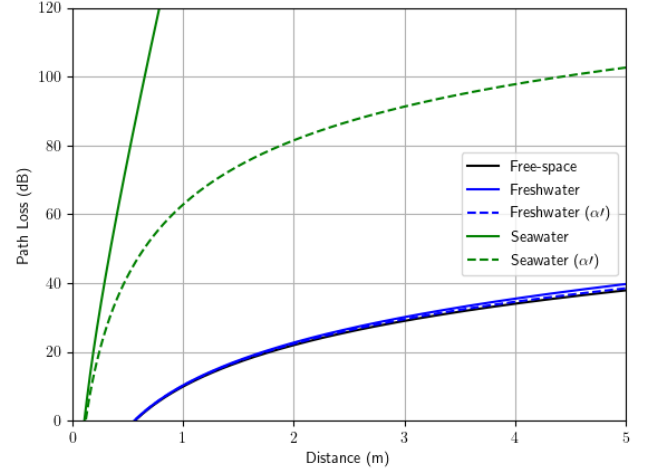

Figure 7. Comparison of path loss for two dipole antennas operating at $f = 13.56\text{MHz}$ using α and $\alpha\prime$.

$$\mathbf{S} = \frac{1}{2} Re(\mathbf{E} \times \mathbf{H}) = \hat{\mathbf{a}}_z \frac{|E_0|}{2} e^{-2\alpha z} Re\left(\frac{1}{\eta_c^*}\right) \tag{20}$$

where η_C is the intrinsic impedance of the medium:

$$\eta_C = \sqrt{\frac{j\omega\mu}{\sigma + j\omega\varepsilon}} \tag{21}$$

For the transmitting antenna in the free-space, S_0 is the power supplied to it over the area of the spread surface:

$$S_0 = \frac{P_{EIRP}}{4\pi z^2} = \frac{P_{TX} G_{TX}}{4\pi z^2} \tag{22}$$

Whereas the radiation power density in a lossy medium is then:

$$S = S_0 e^{-2\alpha z} \tag{23}$$

For the receiving antenna, the average power received is the radiation power density times its effective receiving area A_e [23]:

$$P_{RX} = S \cdot A_e = S \cdot \frac{G_{RX} \lambda^2}{4\pi} \tag{24}$$

The transmission equation then can be written as:

$$P_{RX} = P_{TX} \left(\frac{G_{TX} G_{RX} \lambda^2}{(4\pi z^2)^2}\right) e^{-2\alpha z} \tag{25}$$

where G_{TX} and G_{RX} are the antenna gains for transmitter and receiver respectively, $\lambda = (2\pi)/\beta$ is the wavelength and z is the distance between antennas. This equation assumes that the antennas are aligned and have the same polarization. The path loss PL_{EM} in decibels is then defined as $PL_{EM} = -10\log_{10}(P_{RX}/P_{TX})$.

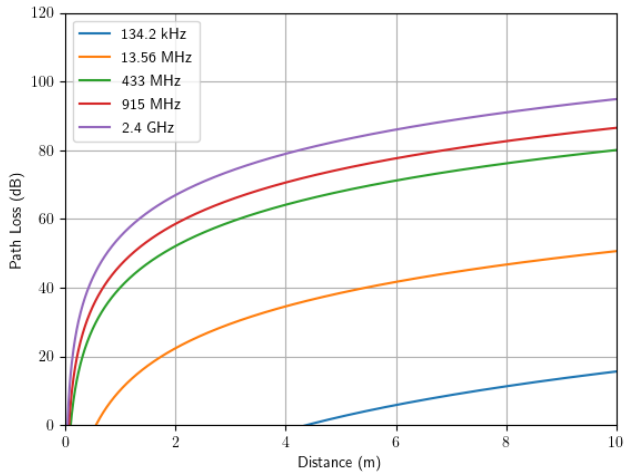Figures 8 and 9 show the path loss of different operating frequencies for a dipole transmitting antenna (reader) and

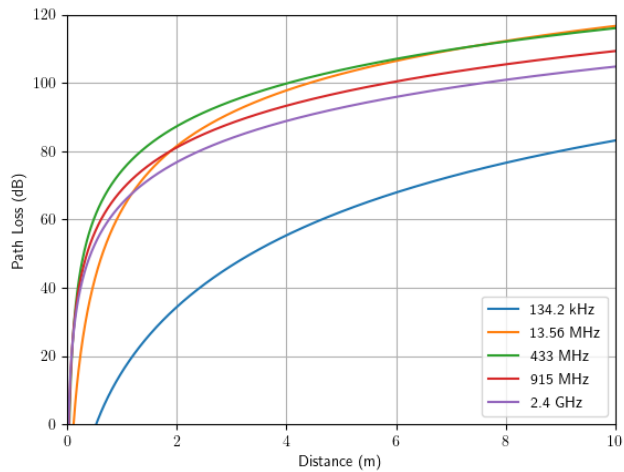Figure 8.   Path loss for RF as a function of distance for two dipole antennas in freshwater using $\alpha\prime$.

Figure 10.   Path loss for RF as a function of frequency for two dipole antennas in freshwater and seawater using $\alpha\prime$.

Figure 9.   Path loss for RF as a function of distance for two dipole antennas in seawater using $\alpha\prime$.

a dipole receiving antenna (tag), both with gain 1.63. For freshwater, it is clear that the higher frequencies suffer more from attenuation than lower frequencies. However, in Figure 9, the path loss increases with the frequency for 134.2 kHz, 13.52 MHz and 433 MHz, after which the path loss starts to stabilise around a region. This happens due to the difference in the behaviour of the propagating medium for different frequencies: the medium can be classified as a good dielectric (insulator) if $(\sigma/\omega\varepsilon)^2 \ll 1$ and – contrastingly – as a good conductor if $(\sigma/\omega\varepsilon)^2 \gg 1$. The frequency at which this behaviour change is around 666 Hz for freshwater ($\sigma = 0.002$ S/m) and 888 MHz for seawater ($\sigma = 4$ S/m). This behaviour can be seen in Figure 10, in which the path loss for a reader and a tag with dipole antennas separated by 50 cm is plotted as a function of the frequency of transmission. In this figure, the path loss for seawater peaks at around 888 MHz.

Data transmission from tag: For passive RFID, the method of transmitting back to the reader is via *Backscatter*. Electromagnetic waves are reflected by objects that are larger than half the wavelength ($\frac{\lambda}{2}$)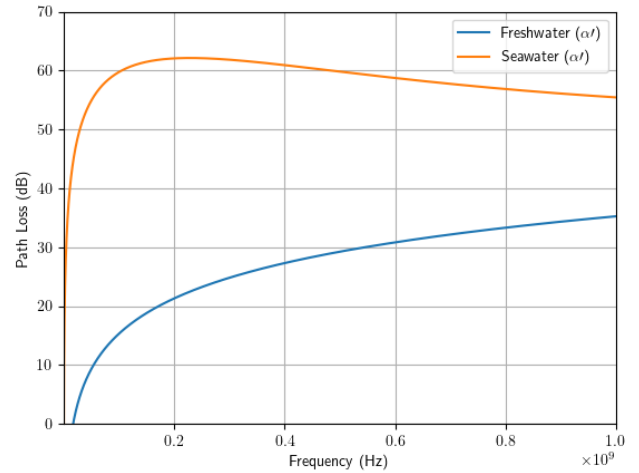. The efficiency of this reflection depends on the reflection cross-section of the object: antennas that are resonant with the waves have a larger reflection cross-section. The reflection characteristics can be altered by changing the load that is connected to the antenna. For example, if a load R_L is switched on and off while connected to the antenna, this changes the reflection characteristics of the antenna, generating a modulated backscatter signal [17]. The range is limited by the amount of energy that reaches the tag (path loss) and the sensitivity of the reader's receiver to the reflected signal (reflected signal strength $\propto 1/x^4$) [24]. The authors in [25] present a method for measuring the backscatter of an RFID tag and for calculating its radar cross-section. They utilise a network analyzer connected to an anechoic chamber.

V. MEASUREMENTS

To explore the difference in magnetic field strength between free-space and water in the near-field region, a preliminary experiment was designed. The Anritsu MS2038C VNA Master [26] vector network analyser and the probe 100C from Beehive Electronics, USA [27] were used to measure the magnetic field strength at the system's resonant frequency. Two Evaluation Kit RFID readers were used: *MRD2EVM* from Texas Instruments, USA that operates at 134.2 kHz [28] and *Pepper Wireless C1 USB* from Eccel Technology Ltd, UK that operates at 13.56 MHz [29]. Both have square loop antennae embedded on the printed circuit board, with sides of length 3.0 cm and 4.5 cm, and number of turns 5 and 1, respectively.

For a square loop antenna with N-turns, the magnetic field strength in free-space can be written as [30]:

$$H_0 = \frac{NI}{2\pi \left(\frac{z^2}{l^2} + \frac{1}{4}\right)\sqrt{z^2 + \frac{l^2}{2}}} \qquad (26)$$

Where z is the distance from the centre of the antenna and l is the length of the side of the antenna. Using 7, for a lossy medium (in this case freshwater), the magnetic field strength is then $H = H_0 exp(-\alpha z)$. Using α from I we can then calculate the theoretical values for the magnetic field strength for any

distance and compare this with the measurements made with the probe.

For both systems, the setup for the experiments was the same, as seen in Figure 11. The probe was placed in different distances z from the centre of the embedded antenna of the reader. The free-space tests were done without the water container, while the freshwater measurements were done using a plastic container bigger than the antenna filled with tap water. The plastic container was then placed touching the antenna, and the probe was submerged in the water to get the measured field strength.
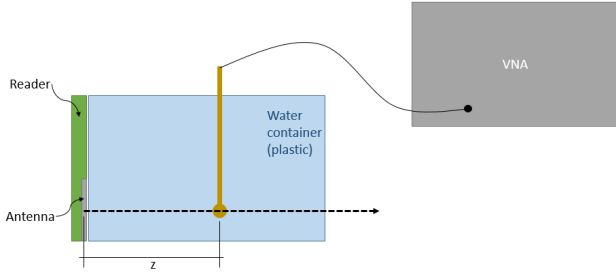

Figure 11. Experiment setup for measuring the magnetic field strength in water.

Figure 12 shows the theoretical and measured values for the 134.2kHz system, while Figure 13 shows the values for the 13.56MHz system. We can see that for both cases the measured values agree with the calculated theoretical ones. The difference between free-space and freshwater for the theoretical values is very small due to the small α for freshwater. However, we can see that the difference between measured field strength in freshwater and free-space is greater. This is could be due to the interfaces of water and plastic and water and air that could introduce losses to the system. For the 13.56MHz system, the attenuation underwater is bigger than the attenuation for the 134.2kHz. This is due to the higher attenuation coefficient α for higher frequencies.
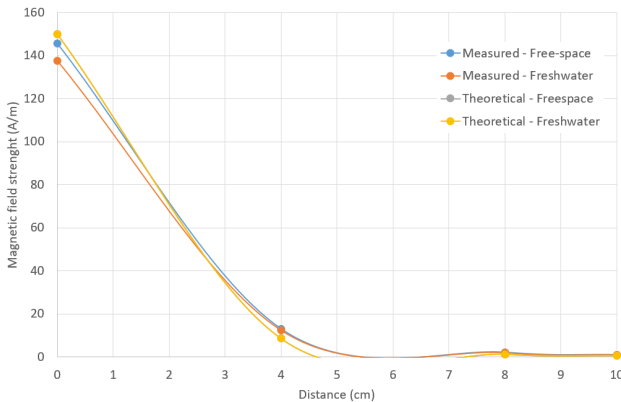

Figure 12. Theoretical and measured field strength values for the Texas Instruments MRD2EVM evaluation kit ($f = 134.2$kHz).

VI. DISCUSSIONS

The most common method of wireless transmission underwater is acoustic communication. This is due to the long
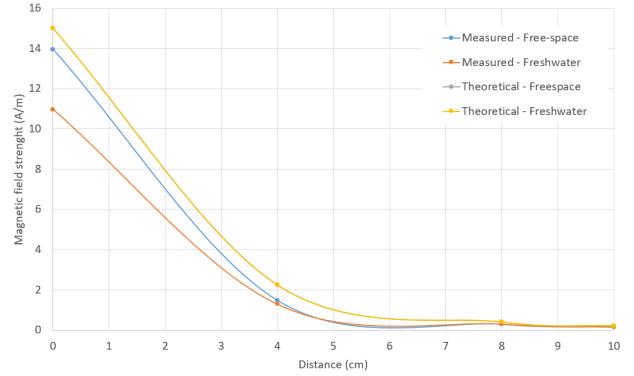

Figure 13. Theoretical and measured field strength values for the Eccel Technology Pepper C1 USB evaluation kit ($f = 13.56$MHz).

range that can be accomplished with this technology. However, some applications do not need such long range and are deeply affected by acoustic noise and refractions, reflections and multipath due to the proximity to the water surface, such as coastal environments. In these cases, wireless communication can be better served by other methods that do not suffer from these problems. We explore the possibility of using RFID technology to better serve these environments.

In the near-field region, the magnetic component of the electromagnetic field dominates. The method of communication for RFID in this region is MI. Compared to other methods of underwater communications, MI has several advantages. It is not affected by multipath propagation or fading and the magnetic field can cross the water to air boundary with low attenuation [12]. The signal propagation delay is negligible if compared to acoustic waves. The channel response is predictable, and a sufficiently large range can be achieved with modest data rates [11].

For the far-field, the electromagnetic field propagates as a wave, and the communication is realised through radio-frequency. Due to the high attenuation, there is a severe constraint on data rates and propagation distances for this method [1]. Lower frequency signals have lower attenuation (due to conductivity of the water) but require larger antennas. This also limits the bandwidth of the system due to the lower frequency of operation. Higher frequency systems would then require more power to reach the same ranges. Shallow water environments, in particular, pose a problem to wave propagation due to the proximity to the water to air upper boundary and to the river/sea bed, which causes multipath propagation [5].

Both technologies do not require line-of-sight and are unaffected by light and acoustic ambient noise. Moreover, the channel response is independent of water quality conditions, such as turbidity. The achievable range for a given transmission power is not great for both methods, as long-range transmissions underwater are best served by acoustic communication. However, the numerical results show that MI has lower attenuation than RF for freshwater, and similar results for seawater, which agrees with other studies such as [12]. Combined with its immunity to multipath and fading, MI is a great alternative for wireless communications underwater.

Added to that, the achievable range of MI communications can be greatly extended by deploying waveguides that do not require power – simple passive relay coils that guide the magnetic field – such as demonstrated in [12][22]. For example, [12] uses an MI waveguide and achieves a range 26 times higher than a normal MI system. Another development that improves MI communications underwater is to use omnidirectional coils that remove the requirement of the transmitting and receiving coils being aligned [11][21].

However, to design an underwater RFID system is to balance a trade-off between range, transmission power and frequency (and therefore data rate and channel capacity). Nonetheless, the RFID system can always be engineered to achieve the best range given its power budget. For an MI system, the size and number of turns of the transmitting and receiving coils has an impact on the path loss. In the far-field category, the antenna can be carefully designed to provide the best radar cross-section, and therefore antenna gain, for the desired application.

An example application that would benefit from MI communication over acoustic would be sensors deployed in coastal areas and fish farms. In these environments, the acoustic noise – from waves, animal life and vessels – and the proximity with the water surface negatively impact acoustic underwater communications. In these cases, MI underwater communication would better fulfil the needs of the system.

VII. Conclusions and Future Work

Given the existing challenges in wireless underwater communications, it is worth exploring alternatives, such as RFID. However, underwater RFID is not a well-explored topic. In this paper, we expanded on the existing theoretical model for RFID channel characteristics to account for the attenuation that the electromagnetic field suffers underwater. The RFID operation was separated into two categories: near-field and far-field. For both cases, the physical characteristics of the transmission were presented and from this, the equation for path loss was obtained and the values for different system configurations were explored.

In both technologies, the water salinity is a problem, as it increases its conductivity and, therefore, its attenuation. However, MI communication has advantages that RF does not have: immunity to multipath propagation and fading. Added to that, the magnetic field can cross the air/water boundary, which is required for some applications. Therefore, near-field RFID communication is a promising alternative for underwater wireless communications.

The model presented in this paper considers that both the transmitting and receiving antennas are located underwater with no transition borders and other losses. This model could be expanded to account for transition borders such as the air-water interface located at the water surface or the interface with the waterproofing material of the reader and tag. In this paper, we also presented some preliminary measurements for magnetic field strength in free-space and freshwater. For future work, we plan to include underwater measurements with water of different salinity values and refine the measurement procedure.

References

[1] C. M. G. Gussen, P. S. R. Diniz, M. L. R. Campos, W. A. Martins, F. M. Costa, and J. N. Gois, "A Survey of Underwater Wireless Communication Technologies," *Journal of Communication and Information Systems*, vol. 31, no. 1, pp. 242–255, 2016, 00018.

[2] J. Heidemann, Wei Ye, J. Wills, A. Syed, and Yuan Li, "Research challenges and applications for underwater sensor networking," in *IEEE Wireless Communications and Networking Conference, 2006. WCNC 2006*. Las Vegas, NV, USA: IEEE, 2006, pp. 228–235, 00974.

[3] M. C. Domingo, "An overview of the internet of underwater things," *Journal of Network and Computer Applications*, vol. 35, no. 6, pp. 1879–1890, Nov. 2012.

[4] L. Lambo, Z. Shengli, and C. Jun-Hong, "Prospects and problems of wireless communication for underwater sensor networks," *Wireless Communications and Mobile Computing*, vol. 8, no. 8, pp. 977–994, Oct. 2008.

[5] X. Che, I. Wells, G. Dickers, P. Kear, and X. Gong, "Re-evaluation of RF electromagnetic communication in underwater sensor networks," *IEEE Communications Magazine*, vol. 48, no. 12, pp. 143–151, Dec. 2010.

[6] A. Pozzebon, "Bringing near field communication under water: Short range data exchange in fresh and salt water," in *2015 International EURASIP Workshop on RFID Technology (EURFID)*, Oct. 2015, pp. 152–156, 00003.

[7] D. Bertoni, G. Sarti, G. Benelli, A. Pozzebon, and G. Raguseo, "Radio Frequency Identification (RFID) technology applied to the definition of underwater and subaerial coarse sediment movement," *Sedimentary Geology*, vol. 228, no. 3, pp. 140–150, Jul. 2010.

[8] E. B. Thorstad, A. H. Rikardsen, A. Alp, and F. Økland, "The Use of Electronic Tags in Fish Research – An Overview of Fish Telemetry Methods," *Turkish Journal of Fisheries and Aquatic Sciences*, vol. 13, no. 5, pp. 881–896, 2013.

[9] S. J. Cooke, S. G. Hinch, M. C. Lucas, and M. Lutcavage, "Biotelemetry and Biologging," in *Fisheries Techniques*, 3rd ed. American Fisheries Society, 2012, pp. 819–860.

[10] G. Benelli and A. Pozzebo, "RFID Under Water: Technical Issues and Applications," in *Radio Frequency Identification from System to Applications*, M. I. B. Reaz, Ed. InTech, Jun. 2013.

[11] I. F. Akyildiz, P. Wang, and Z. Sun, "Realizing underwater communication through magnetic induction," *IEEE Communications Magazine*, vol. 53, no. 11, pp. 42–48, Nov. 2015, 00054.

[12] M. C. Domingo, "Magnetic Induction for Underwater Wireless Communication Networks," *IEEE Transactions on Antennas and Propagation*, vol. 60, no. 6, pp. 2929–2939, Jun. 2012.

[13] B. Gulbahar and O. B. Akan, "A Communication Theoretical Modeling and Analysis of Underwater Magneto-Inductive Wireless Channels," *IEEE Transactions on Wireless Communications*, vol. 11, no. 9, pp. 3326–3334, Sep. 2012, 00080.

[14] Z. Sun and I. F. Akyildiz, "Magnetic Induction Communications for Wireless Underground Sensor Networks," *IEEE Transactions on Antennas and Propagation*, vol. 58, no. 7, pp. 2426–2435, Jul. 2010, 00376.

[15] U. Azad, H. C. Jing, and Y. E. Wang, "Link Budget and Capacity Performance of Inductively Coupled Resonant Loops," *IEEE Transactions on Antennas and Propagation*, vol. 60, no. 5, pp. 2453–2461, May 2012, 00058.

[16] H. Nguyen, J. I. Agbinya, and J. Devlin, "Channel Characterisation and Link Budget of MIMO Configuration in Near Field Magnetic Communication," *International Journal of Electronics and Telecommunications*, vol. 59, no. 3, pp. 255–262, Sep. 2013, 00013.

[17] K. Finkenzeller, *RFID Handbook: Fundamentals and Applications in Contactless Smart Cards, Radio Frequency Identification and near-Field Communication*. Hoboken, N.J.: Wiley, 2014, oCLC: 883259929.

[18] C. A. Balanis, *Advanced Engineering Electromagnetics*, 2nd ed. Hoboken, N.J: John Wiley & Sons, 2012, 08263.

[19] ——, *Antenna Theory: Analysis and Design*, 3rd ed. Hoboken, NJ: John Wiley, 2005, 26986.

[20] H. Lehpamer, *RFID Design Principles*, 2nd ed. Boston: Artech House, 2012.

[21] H. Guo, Z. Sun, and P. Wang, "Channel Modeling of MI Underwater Communication Using Tri-Directional Coil Antenna," in *2015 IEEE Global Communications Conference (GLOBECOM)*, Dec. 2015, pp. 1–6, 00023.

[22] Z. Sun, I. F. Akyildiz, S. Kisseleff, and W. Gerstacker, "Increasing the Capacity of Magnetic Induction Communications in RF-Challenged Environments," *IEEE Transactions on Communications*, vol. 61, no. 9, pp. 3943–3952, Sep. 2013, 00048.

[23] C. Uribe and W. Grote, "Radio Communication Model for Underwater WSN," in *2009 3rd International Conference on New Technologies, Mobility and Security*, Dec. 2009, pp. 1–5, 00039.

[24] R. Want, "RFID Explained: A Primer on Radio Frequency Identification Technologies," *Synthesis Lectures on Mobile and Pervasive Computing*, vol. 1, no. 1, pp. 1–94, Jan. 2006.

[25] K. V. S. Rao and P. V. Nikitin, "Theory and measurement of backscattering from RFID tags," *IEEE Antennas and Propagation Magazine*, vol. 48, no. 6, pp. 212–218, Dec. 2006, 00484.

[26] *VNA Master MS20xxC Technical Data Sheet*, Anritsu, Aug. 2019, version AE.

[27] *100 Series EMC Probes*, Beehive Electronics, 2005, rev. 2.2.

[28] *HDX RFID Reader System – Microreader RI-STU-MRD2*, Texas Instruments, Aug. 2012.

[29] *Pepper C1 User Manual*, Eccel Technology Ltd, Sep. 2019, rev. 1.4.

[30] G. D. Durgin, *ECE 3065 Notes*, TESSAL - Georgia Institute of Technology, Notes on Inductive RFID.